# GOLGA2/GM130 is a novel target of neuroprotection therapy in intracerebral hemorrhage

**shu wen deng**
Second Xiangya Hospital
**Qing Hu**
Second Xiangya Hospital
**Qiang He**
Second Xiangya Hospital
**Xi qian Chen**
Second Xiangya Hospital
**Qiang Lei**
Second Xiangya Hospital
**wei lu** ( luwei0338@csu.edu.cn )
second xiangya hospital https://orcid.org/0000-0001-7376-5029

**Research**

**Keywords:** Golgi apparatus, therapy, intracerebral hemorrhage, autophagy, blood brain barrier

**Posted Date:** March 6th, 2021

**DOI:** https://doi.org/10.21203/rs.3.rs-281611/v1

## Abstract

# Background

Impairment of the blood-brain barrier after intracerebral hemorrhage (ICH) can lead to secondary brain injury and aggravate neurological deficits. Owing in part to our lack of understanding of the mechanism of ICH injury to the blood-brain barrier, there are currently no effective methods to prevent or treat it. Here, we explored the effects of Golgi apparatus protein GM130 overexpression or silencing on the blood-brain barrier and neurological function after ICH, to better understand the mechanism involved and facilitate the development of new therapeutic methods.

# Results

Levels of the tight junction-associated proteins ZO-1 and occludin decreased, while those of LC3-II, a marker for autophagosomes, increased in hemin-treated Bend.3 cells ($p < 0.05$). The levels of ZO-1 and occludin increased, while those of LC3-II decreased with GM130 overexpression ($p < 0.05$). ZO-1 and occludin expression decreased and LC3-II increased after siGM130 transfection, mimicking the effect of hemin ($p < 0.05$). Tight junctions were disconnected after hemin or siGM130 treatment and repaired with GM130 overexpression. siGM130 transfection in Bend.3 cells increased autophagy flux, whereas GM130 overexpression downregulated autophagy flux. Similar results were verified in an *in vivo* ICH model. Perihematomal ZO-1 and occludin expression increased, while LC3-II expression decreased in ICH rats ($p < 0.05$). ZO-1 and occluding expression further decreased and LC3-II expression increased in siGM130-treated ICH rats ($p < 0.05$), whereas a reverse effect was observed in AAV-GM130-treated ICH rats ($p < 0.05$). Perihematomal Evans blue and brain water content were much higher in siGM130-treated ICH rats than in the control ICH rats. AAV-GM130-treated ICH rats showed a lower perihematomal Evans blue and brain water content than the control ICH rats.

# Conclusions

GM130 overexpression can protect the integrity of the blood-brain barrier from brain injury, inhibit excessive autophagy flux in an ICH *in vivo* model, and further improve the neurobehavioral prognosis. GM130 overexpression may mediate tight junction protein repair by directly reducing autophagy flux in an ICH *in vitro* model. GM130 may be a therapeutic target for acute brain injury after ICH.

## Introduction

Spontaneous intracerebral hemorrhage (ICH) is a potentially fatal cerebrovascular disease accompanied by a high mortality rate. Brain injury after ICH can be divided into primary and secondary brain injury [1]. Blood components and blood-cell degradation products from ruptured blood vessels can cause severe secondary brain injury [2]. Blood-brain barrier (BBB) impairment after ICH is an important

pathophysiological mechanism [3]. BBB damage can lead to secondary brain injury and aggravate neurological deficits [4, 5]. In recent decades, no new effective methods have emerged to prevent ICH from injuring the BBB [6]. Therefore, a comprehensive understanding of the mechanism of BBB injury is needed to help in the development of new therapeutic methods.

The BBB is a physical and physiological barrier between blood and the brain, and disruption of the BBB integrity is a well-documented cause of brain edema following a variety of brain injuries [7]. BBB integrity is damaged under oxidative stress and inflammatory conditions. In addition, an increase in autophagy flux after stroke can affect the integrity of the BBB [8], but whether its effect is destructive or protective remains controversial [9, 10]. However, most studies suggest that excessive autophagy may cause destruction of the BBB after ICH [11, 12].

Autophagy is usually enhanced under conditions of starvation, oxidative damage [13], endoplasmic reticulum stress [14] or Golgi stress [15]. Defects in autophagy flux may lead to the accumulation of damaged or aging proteins and play a critical role in the pathogenesis of several diseases, including neurodegenerative diseases [16], cardiovascular diseases [17], metabolic diseases [18], and cancer [19]. Excessive autophagosome formation is induced by stress conditions, such as oxidative stress, energy and nutrient deprivation, and pro-apoptotic conditions. It can also be regulated by Golgi structure proteins, such as GM130 and Grasp55.

GM130 is a cis-Golgi protein that plays a role in maintaining Golgi morphology and controlling protein glycosylation and vesicle transport. Inhibition of glycosylation caused by silencing of GM130 can induce autophagy [20]. Further studies revealed that GM130 regulates the autophagy signaling pathway by interacting with GABARAP [21, 22]. Therefore, GM130 plays a role in maintaining a proper level of autophagy. We previously observed that GM130 decreased and the Golgi became fragmented in an ICH *in vivo* model [23]. However, the specific role of GM130 in the pathogenesis of ICH is unknown. Based on the above, we hypothesize that targeted regulation of GM130 expression may be able to save the integrity of the BBB, which is mediated by influencing autophagy flux, to reduce secondary brain injury and neurological deficits after ICH. Our findings will provide a new treatment direction for BBB protection after ICH.

# Results

### Hemin downregulates GM130 expression, resulting in Golgi dysfunction, destroyed tight junction integrity, and autophagy induction in mouse brain endothelial cells

Hemolysis after ICH leads to the release of hemoglobin, which is further broken down into heme or its oxidized form, hemin [24]. Hemin has been used to mimic ICH *in vitro*. We assessed GM130 expression and Golgi morphology after hemin treatment for 48 h. As shown in Fig. 1a **and b**, GM130 decreased with increasing concentrations of hemin, and at 100 μmol/L of hemin the decrease in GM130 was significant ($p = 0.007$). Immunofluorescence revealed that GM130-marked Golgi apparatus were dispersed in the cytoplasm, and some of them even underwent fragmentation after treatment with hemin (Fig. 1c). Hemin

(100 μmol/L) also significantly decreased the levels of ZO-1 ($p = 0.017$) and occludin ($p = 0.007$) (Fig. 1a **and b)**. Finally, immunofluorescence showed that tight junctions became discontinuous.

LC3-II increased ($p = 0.001$) and p62 decreased ($p = 0.006$) after hemin treatment (100 μmol/L) compared with that of untreated cells, indicating elevated autophagy (Fig. 1a **and b)**. Using transmission electron microscopy (TEM), we also observed the formation of more autophagosomes after hemin treatment (Fig. 5).

### GolGA2/GM130 overexpression reduces autophagosome formation and repairs tight junction integrity and Golgi morphology in Bend.3 cells

To confirm the role of GM130 in autophagy and tight junction integrity, we transfected Bend.3 cells with either a pcDNA3.1 empty vector or pcDNA3.1-GM130. After a 12 h incubation, cells were treated with hemin for 48 h. As shown in Fig. 2a **and c**, GM130 was successfully overexpressed in both vehicle- and hemin-treated Bend.3 cells. GM130 overexpression inhibited autophagosome formation with decreased LC3b ($p = 0.028$) and increased p62 ($p = 0.042$); however, it improved the expression of occludin ($p = 0.047$) and ZO-1 ($p = 0.027$) in pcDNA3.1-GM130 treated Bend.3 cells (Fig. 2a **and b)**. In addition, GM130 overexpression repaired tight junction integrity in hemin-treated Bend.3 cells (Fig. 2d). Immunofluorescence showed that tight junction proteins were more continuous in GM130-overexpressing cells than in empty-vector cells (Fig. 4a **and b).**

Compared with the empty vector-treated cells with hemin, LC3-II significantly decreased ($p = 0.023$), whereas p62 increased ($p = 0.019$) in GM130-overexpressing cells with hemin **(Fig. 2ca and d)**. Furthermore, we detected the formation of autophagosomes by TEM. As shown in Fig. 5b, GM130 overexpression reduced the formation of autophagosomes induced by hemin administration and thus, repaired the integrity of tight junctions and Golgi morphology induced by hemin in Bend.3 cells.

## Downregulation of GolGA2/GM130 induces autophagy formation and tight junction disruption in Bend.3 cells

We first examined the silencing efficiency of two different small interfering RNA (siRNA) constructs against GOLGA2/GM130, using western blotting of proteins from Bend.3 cells. siGOLGA2 significantly decreased GOLGA2/GM130 protein levels compared to the negative control ($p < 0.05$) (Fig. 3a**).** There was no obvious difference in cell viability between the negative control (siCtrl) and the siGM130-1 or siGM130-2 group ($p < 0.05$). Next, we used immunofluorescence analysis of GM130 to assess Golgi structure. The structure of the Golgi apparatus varied from a compact, perinuclear distribution to a dispersed distribution throughout the cytoplasm (Fig. 4a). These results indicate that GM130 plays an important role in the maintenance of Golgi structure.

To determine whether GOLGA2/GM130 downregulation has a regulatory role in autophagy and tight junction integrity, western blotting of LC3 and tight junction proteins was performed in siGOLGA2-treated cells. siGOLGA2/GM130 transfection in Bend.3 cells significantly increased LC3-II ($p = 0.001$) and

decreased p62 ($p < 0.001$) compared with the scrambled siRNA control (Fig. 3b **and c).** Furthermore, an increase in autophagosomes was confirmed by TEM in the cytoplasm of GOLGA2/GM130-downregulated cells (Fig. 5a). In addition, siGM130 significantly decreased the levels of tight junction proteins, including occluding ($p = 0.008$) and ZO-1 ($p = 0.016$) (Fig. 3b **and c**). Immunofluorescence of both GM130 and occludin revealed that tight junctions became discontinuous after siGM130 transfection (Fig. 4a). Hemin triggers GM130-mediated Golgi stress, presenting as Golgi morphology alterations, which can mimic the administration of siGM130.

### Disrupted tight junction integrity induced by siGM130 is partially derived from excessive activation of the autophagy pathway

As mentioned before, siGOLGA2/GM130 induced the formation of autophagosomes and BBB disruption. To further investigate whether the mechanism behind the negative regulation by siGM130 on tight junction disruption was mediated by excessive activation of the autophagy pathway, 3-methyladenine (3-MA, a general autophagy inhibitor) was administered to siGM130-transfected cells, and western blot analysis of tight junction proteins was performed. LC3-II significantly decreased ($p = 0.047$) and p62 increased ($p = 0.005$) in siGM130-transfected cells treated with 3-MA ($p < 0.05$) (Fig. 6a). The protein levels of both occludin ($p = 0.023$) and ZO-1 ($p = 0.027$) were elevated in siGM130/3-MA-treated cells than cells treated with only siGM130 (Fig. 6b). 3-MA treatment partially restored the protein levels of occludin and ZO-1, demonstrating that the disruption of tight junctions induced by siGM130 is partially derived from excessive activation of the autophagy pathway.

## GM130 overexpression reduces BBB permeability, alleviates brain edema, and improves neurologic outcomes after ICH

To determine the effect of siGM130 on BBB integrity and neurological function after ICH, siGM130 or scrambled siRNA control was transfected via injection into the lateral ventricles of rats using a stereotactic technique before the animal models were established. Twenty-four hours after transfection, collagenase was administered into the basal ganglia of Sprague-Dawley rats to establish an ICH *in vivo* model. All the following tests were performed 48 h after establishing the ICH model. As shown in Fig. 7c, the Garcia score was much lower in siGM130-transfected ICH rats than in rats given the scrambled siRNA control ($p < 0.001$), indicating that siGM130 can further aggravate neurological defects. Evans blue extravasation assay (Fig. 7a **and b**) and the water content of rat brains (Fig. 7d) revealed that the vascular leakage ($p < 0.001$) and dry-wet weight ratio ($p < 0.001$) in siGM130-treated ICH rats were significantly higher than those in rats given the scrambled siRNA control.

Likewise, to explore the effect of GM130 overexpression on the BBB and neurological function after ICH, adeno-associated virus (AAV)-mediated GM130 overexpression was induced in rats before establishing ICH. AAV-GM130 or AAV-Control was injected into the lateral ventricle using a stereotactic technique before the animal models were established. One month later, collagenase was administered into the basal ganglia of rats to establish an ICH *in vivo* model. All tests were performed 48 h after establishing

the ICH model. Contrary to the effect of siGM130 in ICH, GM130 overexpression mediated by AAV-GM130 significantly improved the Garcia score in the AAV-GM130 ICH group compared to that of the AAV-Control ICH group ($p < 0.001$) (Fig. 8c). The Evans blue extravasation assay and the water content of rat brains showed less vascular leakage (Fig. 8a **and b)** and a lower dry-wet weight ratio (Fig. 8d) in the AAV-GM130 ICH group than in the AAV-Control ICH group ($p < 0.001$). Therefore, GM130 overexpression has a neuroprotective effect in ICH by reducing BBB permeability and alleviating neurological defects and brain edema.

# AAV-GM130 has a neuroprotective effect on ICH via repairing the expression of tight junction proteins

We found that when GM130 decreased, tight junction integrity was destroyed, and autophagy formation significantly increased gradually with the length of time of ICH (from 12 to 72 h) ($p < 0.05$) (Fig. 9). Based on this result, we chose 48 h as the time point for collecting brain tissue after ICH. To explore whether AAV-GM130 alleviated tight junction protein disruption and reduced excessive autophagy pathway activation, western blotting was performed around the hematoma in either AAV-GM130- or AAV-control-transfected ICH rats. We first examined whether AAV-GM130 was successfully transfected into the rat brain (Fig. 10c). Western blotting showed that tight junction proteins (ZO-1 and occludin) significantly increased in AAV-GM130 ICH rats compared to that in AAV-control rats ($p < 0.01$) (Fig. 10a **and b)**. Double immunofluorescent labeling of GM130 and occludin revealed that occludin was more widely distributed in AAV-GM130 ICH rats (Fig. 11). To explore the underlying mechanism of AAV-GM130 in repairing the expression of tight junction proteins, we further detected the expression levels of LC3-II and p62. Figure 10 shows that LC3-II decreased and p62 increased in AAV-GM130 ICH rats ($p < 0.01$). Immunofluorescence showed a smaller distribution of autophagosomes in the AAV-GM130 group than in the AAV-control group (Fig. 12).

In contrast to the neuroprotective effect of GM130 overexpression, silencing of GM130 promoted the formation of autophagosomes and impaired tight junction proteins in hemorrhaged rat brains compared with the negative siRNA control. We first examined whether siGM130 was successfully transfected into the rat brain (Fig. 13c). According to the result, siRNA-1 was selected for subsequent experiments. Western blotting results showed that tight junction proteins (ZO-1 and occludin) decreased and LC3-II increased in siGM130-transfected ICH rats ($p < 0.01$) (Fig. 13a **and b)**. Double immunofluorescent labeling of GM130 and occludin showed that occludin was further fragmented after silencing GM130 in the ICH group (Fig. 14).

# Discussion

Therapies targeted at protecting the integrity of the BBB can reduce neurological defects induced by ICH [3]. In this study, we explored the role of GM130 in BBB protection. We found that regulation of GM130 can protect the integrity of the BBB by maintaining autophagy flux at a proper level and alleviating neurological defection after ICH.

The BBB acts as a physical and physiological barrier that protects the brain from toxic substances. BBB damage results in brain edema and prompts an inflammatory response. Our study found that tight junction proteins were further damaged with the prolongation of ICH. The BBB was destroyed, accompanied by brain edema and neurological dysfunction 48 h after ICH, which is consistent with previous studies [25]. Many signaling factors can control BBB permeability by regulating its structural components, such as inflammatory factor MMP-9 [26] and vascular endothelial growth factor [27] etc. In addition, activation of the autophagy signaling pathway also regulates the BBB [28].

Autophagy is a tightly regulated process for the bulk removal of degraded cytoplasmic macromolecules and organelles in mammalian cells via lysosomes, thus maintaining cell homeostasis [29]. A previous study demonstrated that the higher the level of autophagic neurons in patients with ICH, the greater the severity of neuronal dysfunction [30]. In our study, elevated LC3-II and decreased p62 in the ICH rat brain indicated excessive autophagy flux induced by brain injury. Moreover, the negative regulatory effect on tight junction proteins induced by silencing GM130 in Bend.3 cells could be reversed by administering an autophagy signaling pathway inhibitor. Therefore, inhibition of autophagosome formation can reduce BBB injury induced by excessive autophagy.

Autophagy can be influenced by Golgi dysfunction. As a signaling platform, the Golgi provides not only a membrane for autophagosome formation but also a location for induction and elongation of autophagosomes [15]. Moreover, Golgi-related proteins directly participate in autophagosome formation [15]. In our ICH *in vivo* models, LC3-II expression around the hematoma in the AAV-GM130 group was lower than that in the negative control group. The level of perihematomal LC3-II in the siGM130-transfected group was higher than that of the negative control group. Similar results were also observed in ICH *in vivo* models. These results indicate that GM130 also has a negative regulatory effect on autophagy in ICH models both *in vivo* and *in vitro*, which is similar to previous studies [20].

Golgi fragmentation and decreased GM130 were found in the brains of ICH rats, which is associated with Golgi stress [23]. Golgi dysfunction derived from Golgi stress may be an essential process in the development of disruption in several cell signaling transduction pathways, including the autophagy signaling pathway [31]. Based on these results, we hypothesize that the excessive autophagy signaling induced by decreased GM130 further disrupts the integrity of the BBB and promotes brain edema in ICH. Our study demonstrated that tight junction disruption and autophagy flux increased in the siGM130-transfected ICH group compared to that of the vehicle control ICH group. Moreover, further mechanistic study *in vitro* showed a higher level of occludin and ZO-1 in 3-MA-treated cells compared with that of control cells, demonstrating that 3-MA can partially restore tight junction protein damage induced by the administration of siGM130 in Bend.3 cells. The above result is consistent with our assumption. Furthermore, AAV-GM130-treated ICH rat models showed higher levels of tight junction proteins, lower Evans blue staining, and lower perihematomal brain water content than that of the negative control ICH rat models. Therefore, targeted upregulation of GM130 may be a potential therapy for ICH.

In summary, our study suggests that GM130 overexpression is beneficial for promoting tight junction integrity repair and improving neurobehavioral recovery in ICH rats by directly modulating its downstream targets in the autophagy pathway. GM130 may be a therapeutic target for acute brain injury after ICH.

## Materials And Methods

# Experimental design

Experimental designs are illustrated in Fig. 15. In the first experiment, Bend.3 cells were sorted into 6 groups and treated with various concentrations of hemin (12.5 μmol/L, 25 μmol/L, 50 μmol/L, 100 μmol/L, and 200 μmol/L) to study the expression of GM130, LC3b, p62, occludin and ZO-1 after ICH *in vitro*. Subsequently, Bend.3 cell line was transfected with two types of siRNAs targeting pcDNA3.1-GM130 or GOLGA2/GM130 to check the effect of regulating GM130 on the expression of P62, LC3b, occludin and ZO-1 in normal state or ICH. Lastly, Bend.3 cell line was treated with autophagy inhibitor 3-MA after transfection with siRNA targeting GOLGA2/GM130 and investigated the expression of occludin and ZO-1.

In the second experiment, 30 rats were used (31 rats suffered during surgery, 30 rats survived) to quantify the effects of collagenase on the early brain injury post ICH. The rats were randomly and evenly assigned into five groups, each contain 6 rats; sham group, ICH groups at various time points including 12h, 24h, 48h, and 72h.

In the third experiment, 162 rats are used (162 of 170 rats survived after the surgery) to know the effects of siGM130 or AAV-GM130 on early brain injury following ICH at 48h. In the first part, the rats were randomly divided into five groups (sham group, ICH group, ICH + vehicle-1 (transfection reagent) group, ICH + negative control (NC) siRNA group [mixtures of transfection reagent and siRNA diluent], ICH + siGM130 group. In the second part, the rats were randomly divided into four groups (sham group, ICH group, ICH + AAV-NC group, ICH + AAV-GM130 group,). Garcia score (n = 6), brain water content (n = 6), Evans blue extraction analyses (n = 3) and immunoblotting analyses (n = 6) and IF staining analyses (n = 3) were performed for each rat.

# Cells and cell culture

Mouse brain endothelial cells (Bend.3) were purchased from Shanghai Zhong Qiao Xin Zhou Biotechnology company (ZQ-0090) [32]. Cells were cultured in Dulbecco's modified Eagle medium (DMEM; Life Technologies; cat#12900017) with 10% FBS (GIBCO) and 1% PS (100 mg/mL penicillin, 100 mg/mL streptomycin) at 37℃ and provided with 5% CO2 [33]. Hemin (Sigma-51280) dissolved in sodium hydroxide which was then diluted with DMEM administrated in Bend.3 cells to established the ICH model *in vitro*.

# Animal model

The study has been conducted following the guidelines of the Central South University for the care and use of laboratory animals.

The experiment protocol is approved by Central South University Animal Care and Use Committee. SD-rats were housed at 25℃ temperature with access to water and food ad libitum. The light in the room is controlled in a 12-h light/dark cycle [5]. SD-rats were randomly assigned to each group.

Rats were anesthetized with pentobarbital sodium (45 mg/ kg) via intraperitoneal injection and then placed in stereotaxic apparatus. The Collagenase type IV (0.2 U in 1 μl sterile normal saline) was injected into the right basal ganglia of the rat brain with stereotaxic coordinates at AP: 0.1 mm, ML: 3 mm, and DV: 6.0 mm to the bregma [34]. The sham-operated rats were administrated with sterile normal saline. The rats were then allowed to recover separate cages with free access to food and water.

**RNAi-mediated GM130 silencing**in Vitro

Before induction of ICH *in vitro*, cells were transfected with GM130 siRNA duplex 01 (siGM130-1, GenePharma) or GM130 siRNA duplex 02 (siGM130-2, GenePharma) or negative control (NC) siRNA with PepMute (SignaGen). Cells in vehicle group received equal volume of DEPC water. For Western blot or Immunofluorescence, cells were harvested after 72 h of transfection.

**Plasmid construction and transfection**in Virto

The GM130 gene cloned into pcDNA3.1(+) has been extracted from Bend.3 cells and then pcDNA3.1-GM130 was constructed to express GM130. The GM130 PCR primers are as follows: 5’ -ccaagctggctagc gctagcATGTGGCCCCCCCGCTTCCC-3’ and 5’ -gtttaaacgggc cctctagaTTATACAACCATGATCTTCA-3’ [32]. The transfection was performed using Lipofectamine 3000 (Invitrogen; cat#L3000150) following manufacturer’s instructions. At 12 h after transfection, Bend.3 cells were treated with hemin for 36 h. Cells are harvested for WB or immunofluorescence after 72 h of transfection.

**siRNA transfection and AAV injection**in Vivo

Prior to the induction of ICH in *vivo*, siGM130 or negative control siRNA (siRNA-NC) (20 μM; GenePharm, Shanghai, China) were mixed with EntransterTM-in vivo (Engreen, Beijing, China). The mixture with a final volume of 5 μl was injected into the right lateral ventricle (stereotaxic coordinates: AP: 0.8 mm, ML: 1.5 mm right to the bregma, and 4.5 mm ventral to the skull) at a flow rate of 0.5 μl/min through another 1 mm burr hole [34]. The rats in negative control-1 group received an intracerebroventricular injection of an equal volume of the transfection reagent before the establishment of ICH. The sham-operated rats were administrated with 5 μl sterile normal saline into the same position [1].

At 20th days before the establishment of the ICH model, 2.5 μl Flag-AAV-GM130 and Flag-AAV-NC purchased from Shanghai Genechem Co., Ltd. ($3\times10^{11}$ viral genomes (vg)/mL) are injected by intracerebroventricular injection. The sham-operated rats were administrated with 2.5 μl sterile normal saline into the same position.

# Evaluation of BBB permeability

Evans Blue (EB) extravasation has been performed as reported previously [35]. 2% solution of EB in normal saline (4 ml/kg) had been administrated in into femoral vein at time point of 48h after ICH. The dye was allowed to circulate for 2 h, and then 200 ml of ice-cold PBS was used for trans-cardiac perfusion under deep anesthesia, and collected the right hemisphere of brain. The supernatant of hemorrhaged brain in the right hemisphere was then mixed with equal amount of trichloroacetic acid solution, and incubated at room temperature for 1 h and afterward, the samples were centrifuged for 30 min at 15,000 r/min in 4°C to separate the supernatant for quantification. [36] EB stain results were measured by a spectrophotometer (Thermo Spectronic Genesys 10 UV, Thermo Fischer Scientific Inc., Waltham, MA, USA) at 610 nm and quantified with a standard curve. [36]

# Garcia scores and measurement of brain water contents

We used Garcia's 18-point scale to assess the neurological defection at 48 h after ICH, which was performed by two trained investigators in blind controlled method. Examination of neurological status is performed using the standards listed in Table 1. [37] Measurement of brain water contents were calculated as previous. [36] The calculated method of brain water content is presented as [(wet weight − dry weight)/wet weight] × 100%.

Table 1
Garcia neurological score

| Test | Score | | | |
|---|---|---|---|---|
| | 0 | 1 | 2 | 3 |
| Spontaneous activity (in cage for 5 min) | No movement | Barely moves | Moves but does not approach at least three sides of cage | Moves and approaches at least three sides of cage |
| Symmetry of movement (four limbs) | Left side: no movement | Left side: slight movement | Left side: moves slowly | Both sides: move symmetrically |
| Symmetry of forelimbs (outstretching while held by tail) | Left side: no movement, no outreaching | Left side: slight movement to outreach | Left side: moves and outreaches less than right side | Symmetrical outreach |
| Climbing wall of wire cage | … | Fails to limb | Left side is week | Normal climbing |
| Reaction to touch on either side of trunk | … | No response on left side | Weak response on left side | Symmetrical response |
| Response to vibrissae touch | … | No response on left side | Weak response on left side | Symmetrical response |

# MTT assay and transmission electron microscopy

For detection of cell viability, 3-(4,5-dimethylthiazol-2-yl)-2,5-diphenyltetrazolium bromide (MTT) assay (Sigma-Aldrich) has been used. Absorbance was detected at 450 nm by a Bio-Rad 680 microplate reader (Bio-Rad, Hercules, CA, USA). [38]

Bend.3 cells were fixed in 2.5% glutaraldehyde at 4℃ for 24 h. After treament with 1% OsO4 for 1 h, Bend.3 cells were washed with PBS for 30 min, dehydrated and then embedded in epon-812. [39] Ultrathin sections (40–70 nm) were cut and mounted on pioloform-coated copper grids. Sections were then stained with lead citrate and uranyl acetate and viewed under transmission electron microscopy (TEM) (Hitachi-HT7700, Japan).

# Immunofluorescence and western blot analyses

Immunofluorescence staining has been performed using antibodies of ZO-1 (Invitrogen, Cat # 40-2200), Occludin (Invitrogen, Cat # 33-1500), GM130 (BD Biosciences, Cat# 610822) and LC3b (Abcam, ab48394) as previously described [40]. For immunoblot analysis, protein were separated by 8–10% sodium dodecyl sulfate-polyacrylamide gel electrophoresis (SDS-PAGE) and transferred to polyvinylidene difluoride (PVDF) membranes. Membranes were blocked with TTBS containing 5% skim milk for 1 hour at room temperature and immunoblotting is performed by incubation overnight at 4°C with the corresponding primary antibodies of ZO-1(Invitrogen, Cat # 40-2200), Occludin (Invitrogen, Cat # 33-1500), GM130 (BD Biosciences, Cat# 610822), LC3b (Abcam, Cat # ab48394) and P62 (Abcam, Cat # ab109012).

# Statistical analysis

All the data are calculated and presented as means ± standard deviation (SD). Statistical analyses are performed in GraphPad Prism software (Prism 8.0) and SPSS version 19.0 software (SPSS, Inc., Chicago, IL, USA). Multiple group data are processed by one-way analysis of variance (ANOVA) to compare differences. The homogeneity of variance with LSD-t method, missing variance with Dunnett-t method. $p < 0.05$ is considered significantly different.

# Abbreviations

AAV, adeno-associated virus; BBB, blood-brain barrier; EB, Evans blue; ICH, intracerebral hemorrhage; 3-MA, 3-methyladenine; siRNA, small interfering RNA; TEM, transmission electron microscopy; WB, western blotting.

# Declarations

### Ethics approval and consent to participate

The study was conducted following the guidelines of the Central South University for the care and use of laboratory animals. The experimental protocol was approved by the Central South University Animal Care and Use Committee.

### Consent for publication

Not applicable

### Availability of data and materials

Not applicable

### Competing interests

The authors declare that they have no competing interests.


### Funding

This work was funded by the National Natural Science Foundation of China (#81571181).


### Authors' contributions

SWD performed the experiments and drafted the manuscript. Qing Hu and Qiang He analyzed the data. XQC and QL helped draft the manuscript. WL conceived and designed the study. All authors read and approved the final manuscript.


### Acknowledgements

The authors thank Shilin Luo at Department of Pharmacy, and Histology Laboratory at Department of Pathology for technical support.


## References


1. Zeng, J., et al., *Isoliquiritigenin alleviates early brain injury after experimental intracerebral hemorrhage via suppressing ROS- and/or NF-κB-mediated NLRP3 inflammasome activation by promoting Nrf2 antioxidant pathway.* Journal of Neuroinflammation, 2017. **14**(1).
2. Zhu, H., et al., *Role and mechanisms of cytokines in the secondary brain injury after intracerebral hemorrhage.* Prog Neurobiol, 2019. **178**: p. 101610.
3. Duan, X., et al., *Intracerebral Hemorrhage, Oxidative Stress, and Antioxidant Therapy.* Oxid Med Cell Longev, 2016. **2016**: p. 1203285.
4. Keep, R.F., et al., *Blood-brain barrier function in intracerebral hemorrhage.* Acta Neurochir Suppl, 2008. **105**: p. 73-7.
5. Wang, Z., et al., *Melatonin Alleviates Intracerebral Hemorrhage-Induced Secondary Brain Injury in Rats via Suppressing Apoptosis, Inflammation, Oxidative Stress, DNA Damage, and Mitochondria Injury.* Transl Stroke Res, 2018. **9**(1): p. 74-91.
6. Keep, R.F., et al., *Brain endothelial cell junctions after cerebral hemorrhage: Changes, mechanisms and therapeutic targets.* J Cereb Blood Flow Metab, 2018. **38**(8): p. 1255-1275.

7. Sajja, R.K., S. Rahman, and L. Cucullo, *Drugs of abuse and blood-brain barrier endothelial dysfunction: A focus on the role of oxidative stress.* J Cereb Blood Flow Metab, 2016. **36**(3): p. 539-54.
8. Kim, K.A., et al., *Role of Autophagy in Endothelial Damage and Blood-Brain Barrier Disruption in Ischemic Stroke.* Stroke, 2018. **49**(6): p. 1571-1579.
9. Wang, P., et al., *Autophagy in ischemic stroke.* Prog Neurobiol, 2018. **163-164**: p. 98-117.
10. Yang, Z., et al., *Autophagy Protects the Blood-Brain Barrier Through Regulating the Dynamic of Claudin-5 in Short-Term Starvation.* Front Physiol, 2019. **10**: p. 2.
11. Song, F., et al., *Therapeutic time window and regulation of autophagy by mild hypothermia after intracerebral hemorrhage in rats.* Brain Res, 2018. **1690**: p. 12-22.
12. Zhao, H., et al., *Role of autophagy in early brain injury after subarachnoid hemorrhage in rats.* Mol Biol Rep, 2013. **40**(2): p. 819-27.
13. Filomeni, G., D. De Zio, and F. Cecconi, *Oxidative stress and autophagy: the clash between damage and metabolic needs.* Cell Death Differ, 2015. **22**(3): p. 377-88.
14. Lin, Y., et al., *Cancer and ER stress: Mutual crosstalk between autophagy, oxidative stress and inflammatory response.* Biomed Pharmacother, 2019. **118**: p. 109249.
15. Deng, S., et al., *Golgi Apparatus: A Potential Therapeutic Target for Autophagy-Associated Neurological Diseases.* Front Cell Dev Biol, 2020. **8**: p. 564975.
16. Barthet, V.J.A. and K.M. Ryan, *Autophagy in Neurodegeneration: Can't Digest It, Spit It Out!* Trends in Cell Biology, 2018. **28**(3): p. 171-173.
17. Bravo-San Pedro, J.M., G. Kroemer, and L. Galluzzi, *Autophagy and Mitophagy in Cardiovascular Disease.* Circ Res, 2017. **120**(11): p. 1812-1824.
18. Saha, S., et al., *Autophagy in health and disease: A comprehensive review.* Biomed Pharmacother, 2018. **104**: p. 485-495.
19. Antunes, F., et al., *Autophagy and intermittent fasting: the connection for cancer therapy?* Clinics (Sao Paulo), 2018. **73**(suppl 1): p. e814s.
20. Chang, S.H., et al., *GOLGA2/GM130, cis-Golgi matrix protein, is a novel target of anticancer gene therapy.* Mol Ther, 2012. **20**(11): p. 2052-63.
21. Joachim, J., et al., *Activation of ULK Kinase and Autophagy by GABARAP Trafficking from the Centrosome Is Regulated by WAC and GM130.* Mol Cell, 2015. **60**(6): p. 899-913.
22. Joachim, J. and S.A. Tooze, *GABARAP activates ULK1 and traffics from the centrosome dependent on Golgi partners WAC and GOLGA2/GM130.* Autophagy, 2016. **12**(5): p. 892-3.
23. Qiu, K., et al., *[Effect of butylphthalide on blood-brain barrier after cerebral hemorrhage in SD rats and the mechanisms].* Zhong Nan Da Xue Xue Bao Yi Xue Ban, 2019. **44**(12): p. 1321-1329.
24. Zille, M., et al., *Neuronal Death After Hemorrhagic Stroke In Vitro and In Vivo Shares Features of Ferroptosis and Necroptosis.* Stroke, 2017. **48**(4): p. 1033-1043.

25. Zeng, Z., X. Gong, and Z. Hu, *L-3-n-butylphthalide attenuates inflammation response and brain edema in rat intracerebral hemorrhage model.* Aging (Albany NY), 2020. **12**(12): p. 11768-11780.
26. Wang, R., et al., *Porcine reproductive and respiratory syndrome virus induces HMGB1 secretion via activating PKC-delta to trigger inflammatory response.* Virology, 2018. **518**: p. 172-183.
27. Almutairi, M.M., et al., *Factors controlling permeability of the blood-brain barrier.* Cell Mol Life Sci, 2016. **73**(1): p. 57-77.
28. Zhang, S., et al., *Autophagy- and MMP-2/9-mediated Reduction and Redistribution of ZO-1 Contribute to Hyperglycemia-increased Blood-Brain Barrier Permeability During Early Reperfusion in Stroke.* Neuroscience, 2018. **377**: p. 126-137.
29. Huang, G., et al., *Autophagy is an important action mode for functionalized selenium nanoparticles to exhibit anti-colorectal cancer activity.* Biomater Sci, 2018. **6**(9): p. 2508-2517.
30. Wu, C., et al., *Increased perihematomal neuron autophagy and plasma thrombin-antithrombin levels in patients with intracerebral hemorrhage: An observational study.* Medicine (Baltimore), 2019. **98**(39): p. e17130.
31. Martínez-Menárguez, J., et al., *Golgi Fragmentation in Neurodegenerative Diseases: Is There a Common Cause?* Cells, 2019. **8**(7).
32. He, Q., et al., *Herpes Simplex Virus 1-Induced Blood-Brain Barrier Damage Involves Apoptosis Associated With GM130-Mediated Golgi Stress.* Front Mol Neurosci, 2020. **13**: p. 2.
33. Li, Z., et al., *Inhibition of lncRNA XIST Improves Myocardial I/R Injury by Targeting miR-133a through Inhibition of Autophagy and Regulation of SOCS2.* Mol Ther Nucleic Acids, 2019. **18**: p. 764-773.
34. Xi, T., et al., *miR-27a-3p protects against blood-brain barrier disruption and brain injury after intracerebral hemorrhage by targeting endothelial aquaporin-11.* J Biol Chem, 2018. **293**(52): p. 20041-20050.
35. Chen, Y., et al., *Norrin protected blood-brain barrier via frizzled-4/β-catenin pathway after subarachnoid hemorrhage in rats.* Stroke, 2015. **46**(2): p. 529-36.
36. Zhu, Q., et al., *Aggf1 attenuates neuroinflammation and BBB disruption via PI3K/Akt/NF-κB pathway after subarachnoid hemorrhage in rats.* J Neuroinflammation, 2018. **15**(1): p. 178.
37. Garcia, J.H., et al., *Neurological deficit and extent of neuronal necrosis attributable to middle cerebral artery occlusion in rats. Statistical validation.* Stroke, 1995. **26**(4): p. 627-34; discussion 635.
38. Wang, S., Z. Zhang, and Q. Gao, *Transfer of microRNA-25 by colorectal cancer cell-derived extracellular vesicles facilitates colorectal cancer development and metastasis.* Mol Ther Nucleic Acids, 2021. **23**: p. 552-564.
39. Zhao, H., et al., *Effects of Simulated Microgravity on Ultrastructure and Apoptosis of Choroidal Vascular Endothelial Cells.* Front Physiol, 2020. **11**: p. 577325.
40. Lei, B., et al., *miR-615-3p promotes the epithelial-mesenchymal transition and metastasis of breast cancer by targeting PICK1/TGFBRI axis.* J Exp Clin Cancer Res, 2020. **39**(1): p. 71.

# Figures

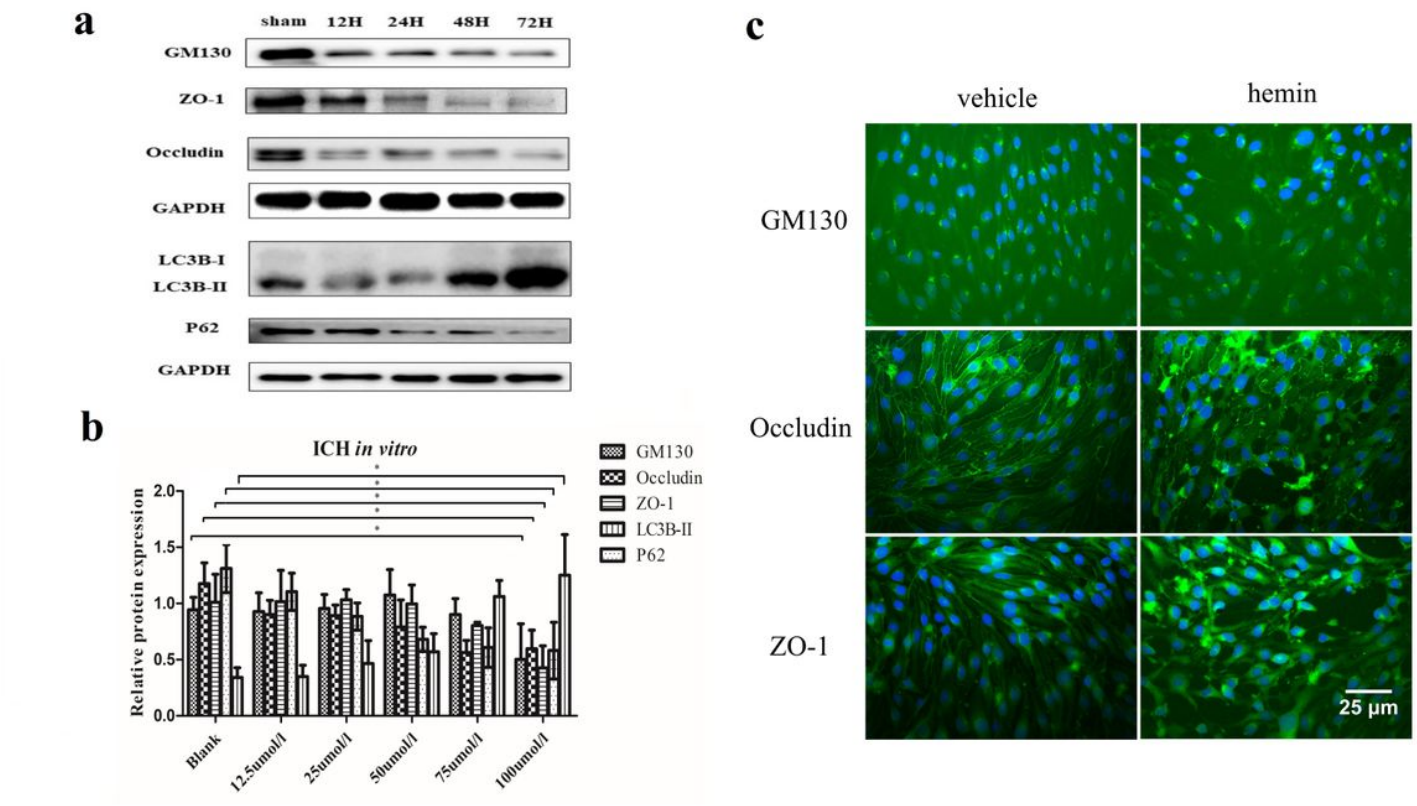


## Figure 1

Hemin downregulates GM130, disrupts Golgi function, destroys tight junction integrity, and induces autophagy. a. GM130, occludin, ZO-1, LC3, and p62 expression in Bend.3 cells of the sham group and different groups treated with several concentrations of hemin (n = 3 per group). b. Quantification data are presented as means ± standard deviation (SD). *p < 0.05. c. Fluorescent imaging showing GM130, occludin, and ZO-1 expression in Bend.3 cells at 48 h after treatment with hemin. Scale bar, 25 μm.

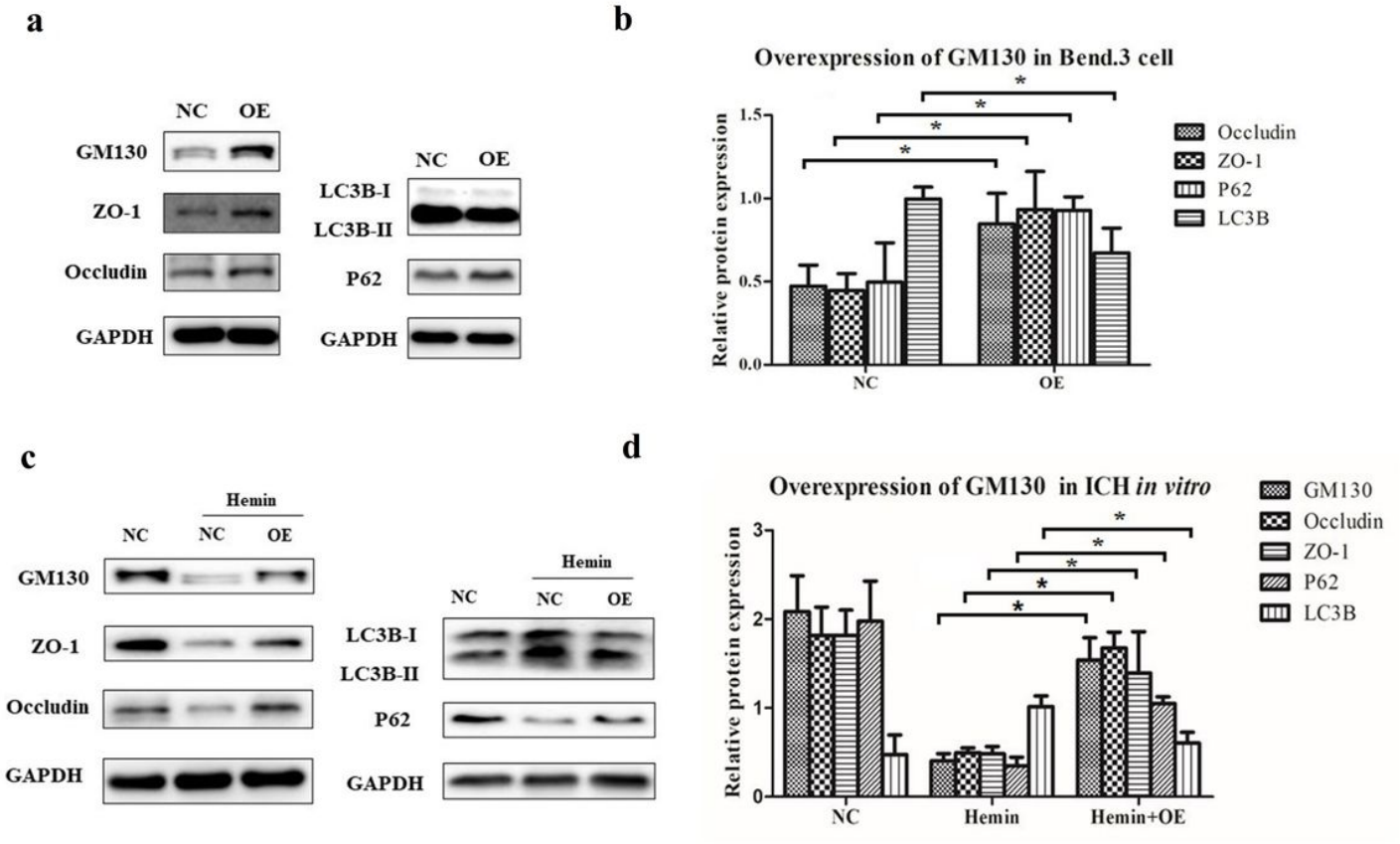


## Figure 2

GolGA2/GM130 overexpression reduces autophagosome formation and repairs tight junction integrity and Golgi morphology. a. Western blot showing GM130, occludin, ZO-1, LC3, and p62 expression in negative-control (NC) and GM130-overexpressing Bend.3 cells (n = 3 per group). c. Western blot showing GM130, occludin, ZO-1, LC3, and p62 expression in NC Bend.3 cells and NC or GM130-overexpressing Bend.3 cells treated with hemin (n = 3 per group). b and d. Quantification data are presented as means ± standard deviation (SD). *p < 0.05.

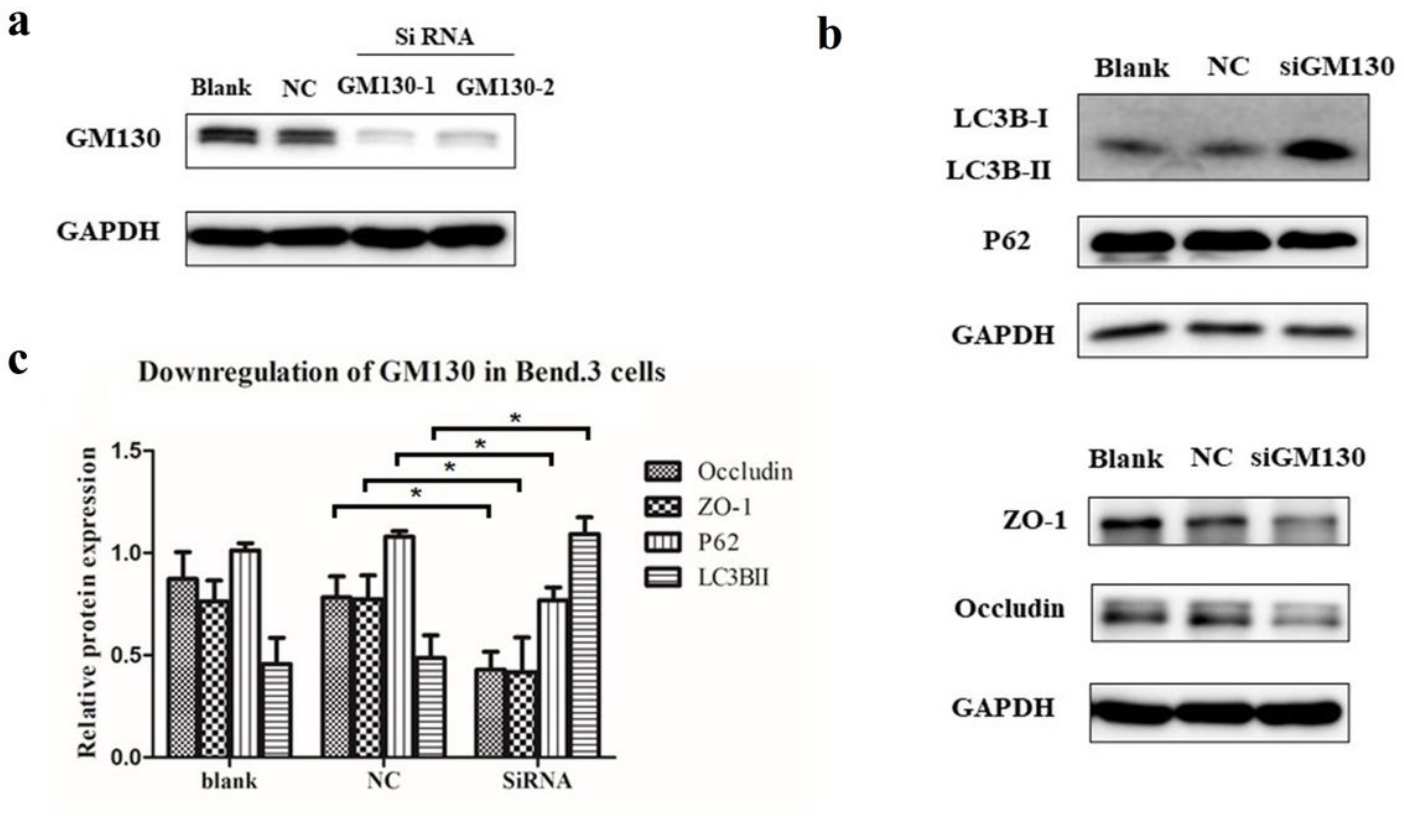


## Figure 3

GolGA2/GM130 downregulation induces autophagy formation and tight junction disruption in Bend.3 cells. a and b. Western blot showing GM130, occludin, ZO-1, LC3, and p62 expression in negative-control (NC) and siGM130-transfected Bend.3 cells (n = 3 per group). c. Quantification data are presented as means ± standard deviation (SD). *p < 0.05.

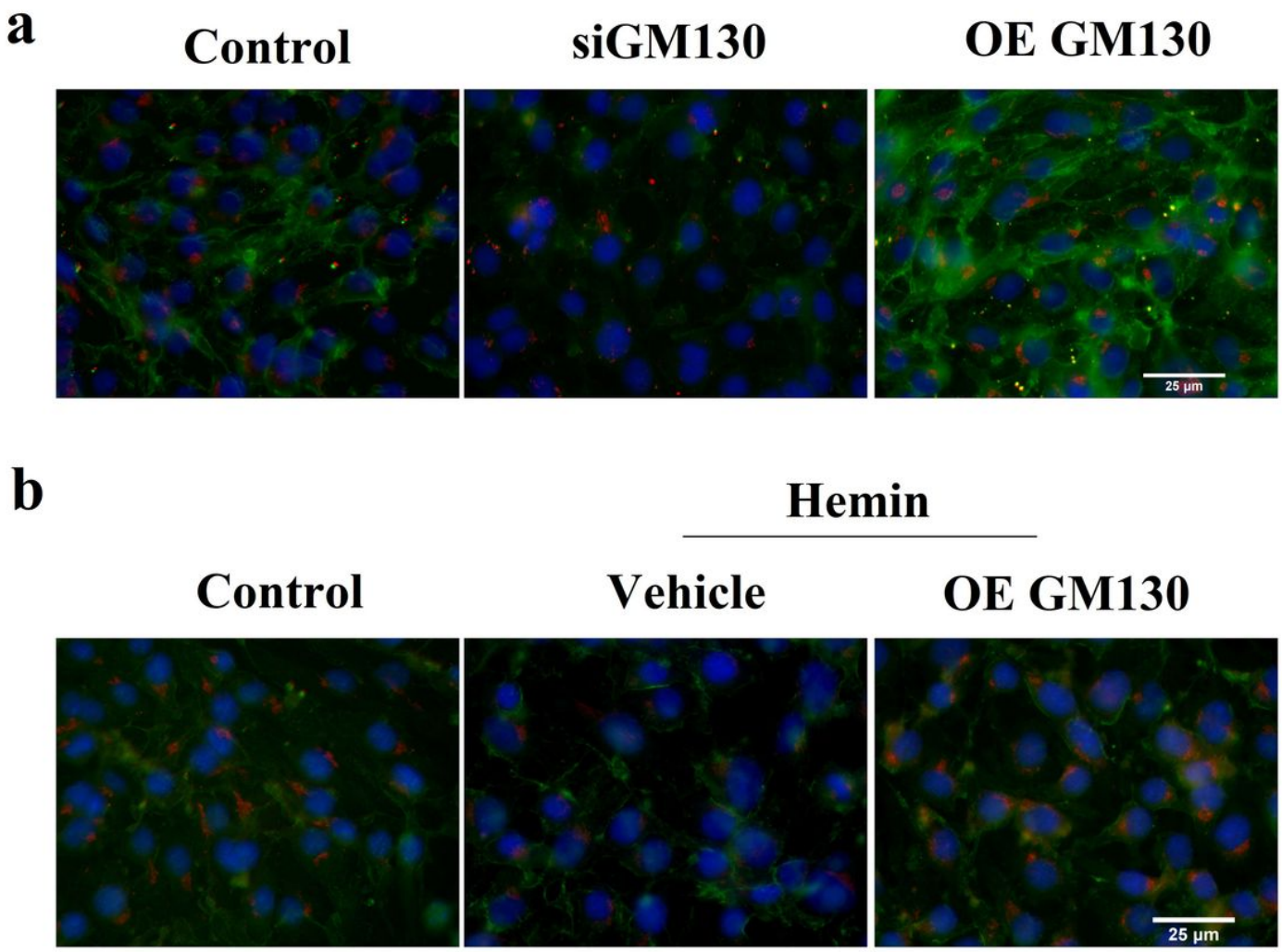


**Figure 4**

Immunostaining of GM130 in Bend.3 cells. a. Immunostaining of GM130 in negative-control (NC), siGM130-transfected, or GM130-overexpressing (OE) Bend.3 cells. b. Immunostaining of GM130 in NC and GM130-OE Bend.3 cells with or without hemin. Scale bar, 25 μm.

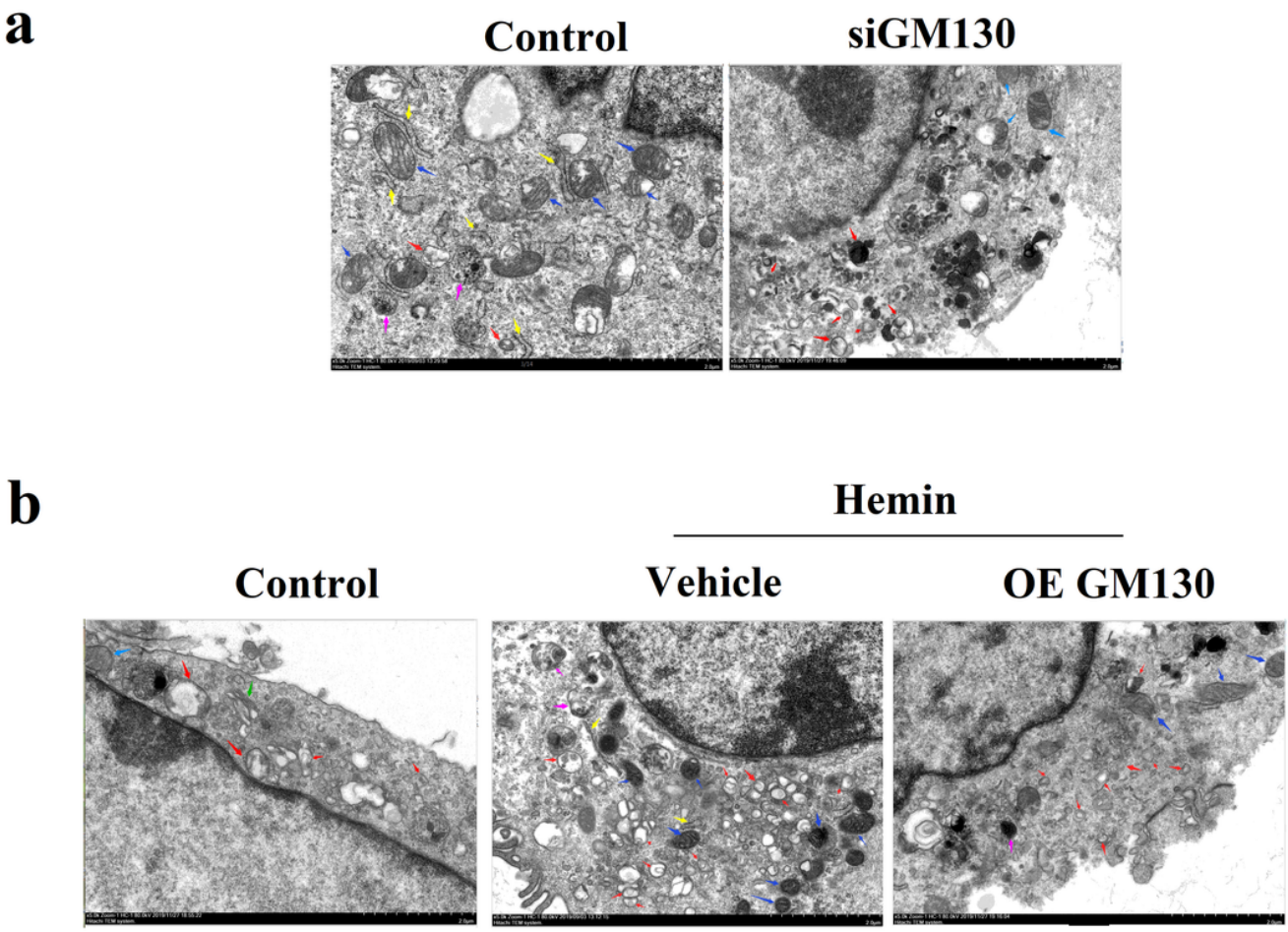


## Figure 5

Transmission electron micrographs of autophagosome formation after hemin treatment. a. Autophagosome formation (red arrow) in negative-control (NC) and siGM130-transfected Bend.3 cells. b. Autophagosome formation (red arrow) in NC and GM130-overexpressing (OE) Bend.3 cells with or without hemin.

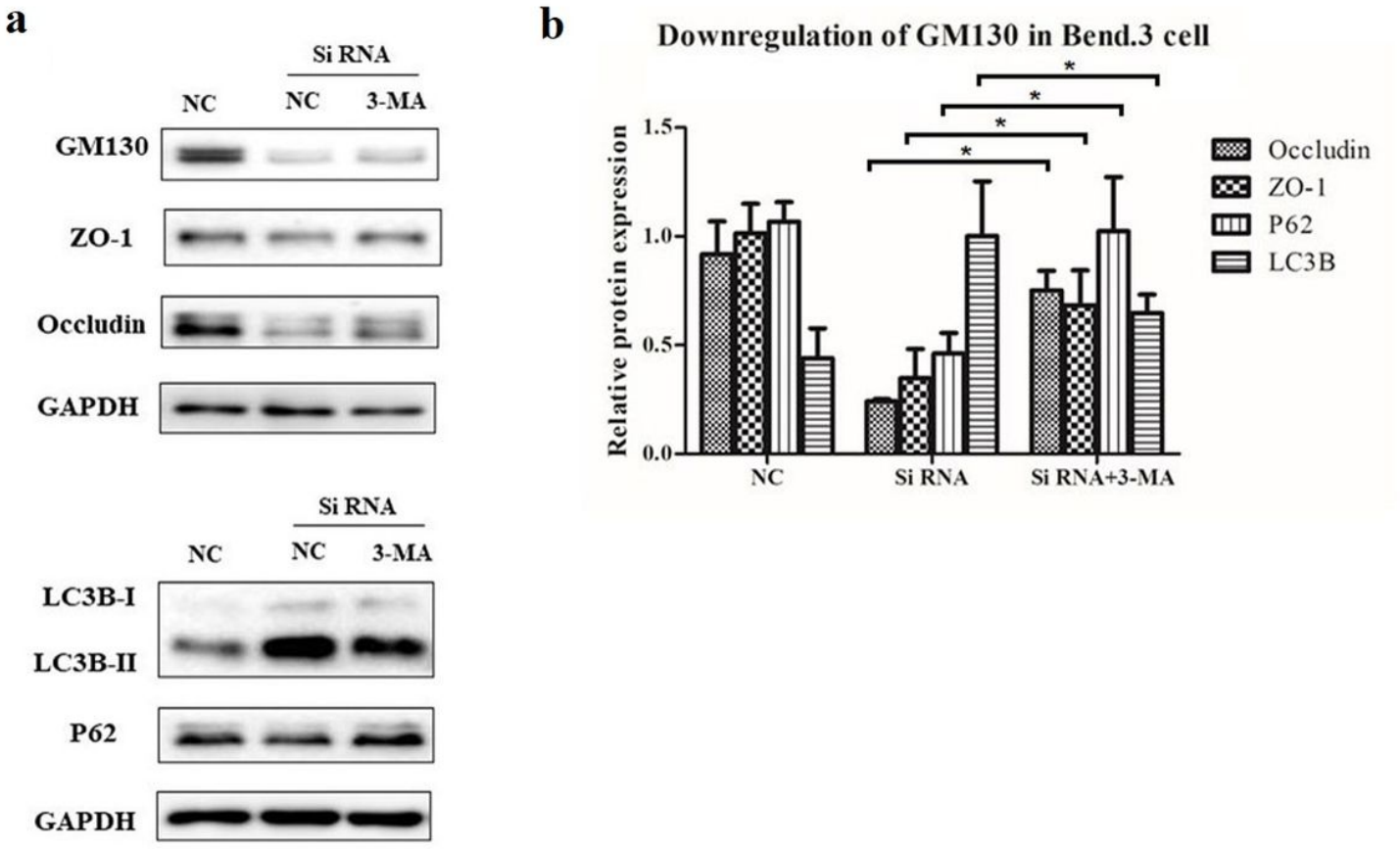


## Figure 6

Excessive activation of autophagy pathway disrupts tight junction integrity induced by siGM130. a. Western blot showing GM130, occludin, ZO-1, LC3, and p62 expression in negative-control (NC) and siGM130-transfected Bend.3 cells with or without autophagy pathway inhibitor (3-methyladenine; 3-MA) (n = 3 per group). b. Quantification data are presented as means ± standard deviation (SD). *p < 0.05.

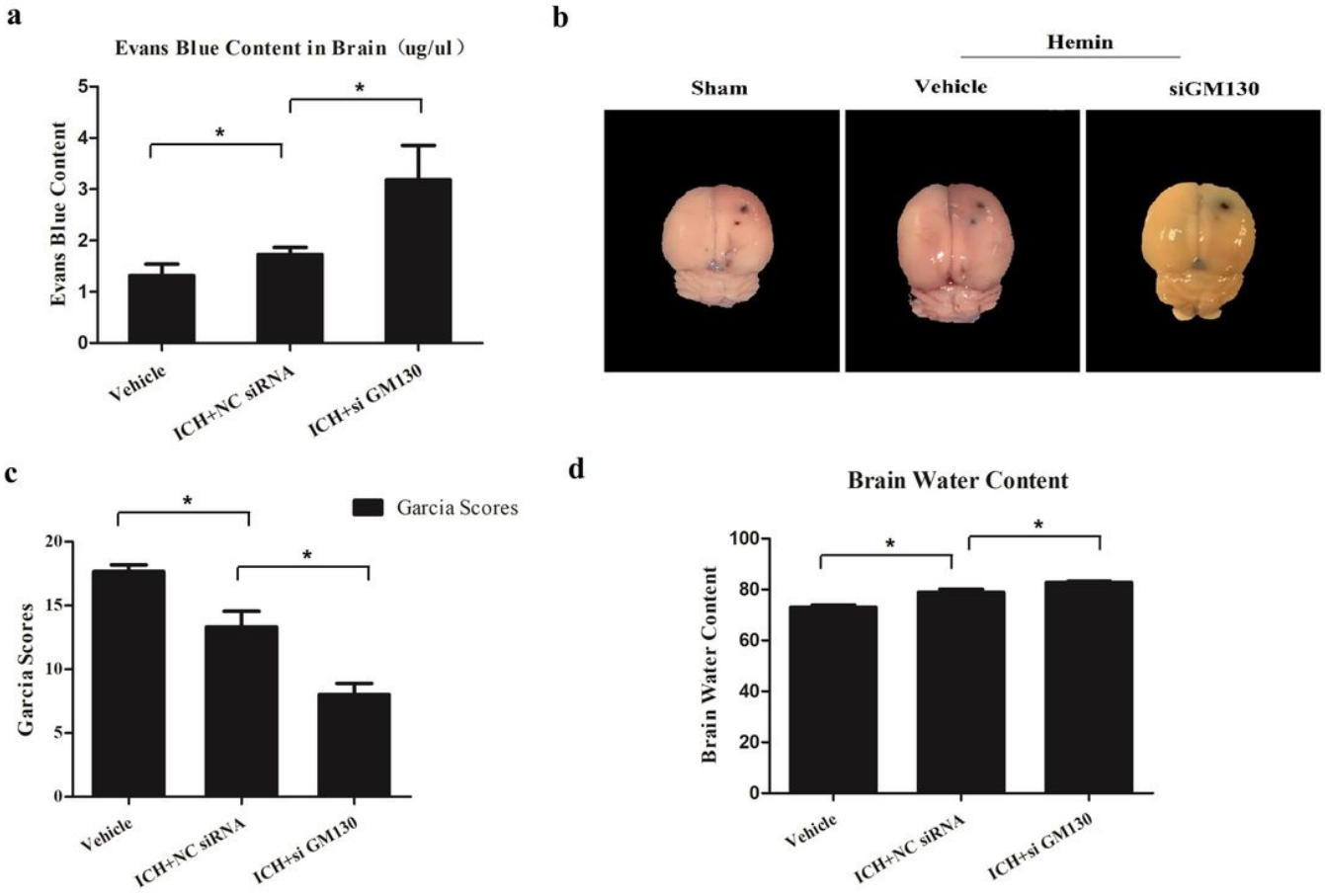


## Figure 7

GM130 overexpression reduces blood-brain barrier permeability, alleviates brain edema, and improves neurologic outcomes after intracerebral hemorrhage. a. Evans blue extravasation assay from the cerebrum of rats (shown in b) from the sham group and intracerebral hemorrhage (ICH) group pre-treated with or without AAV-GM130 (n = 3 per group). c. Garcia score in sham and ICH groups pre-treated with or without AAV-GM130 (n = 6 per group). d. Water content in sham and ICH groups pre-treated with or without siGM130 (n = 6 per group). Data are presented as means ± standard deviation (SD). *p < 0.05.

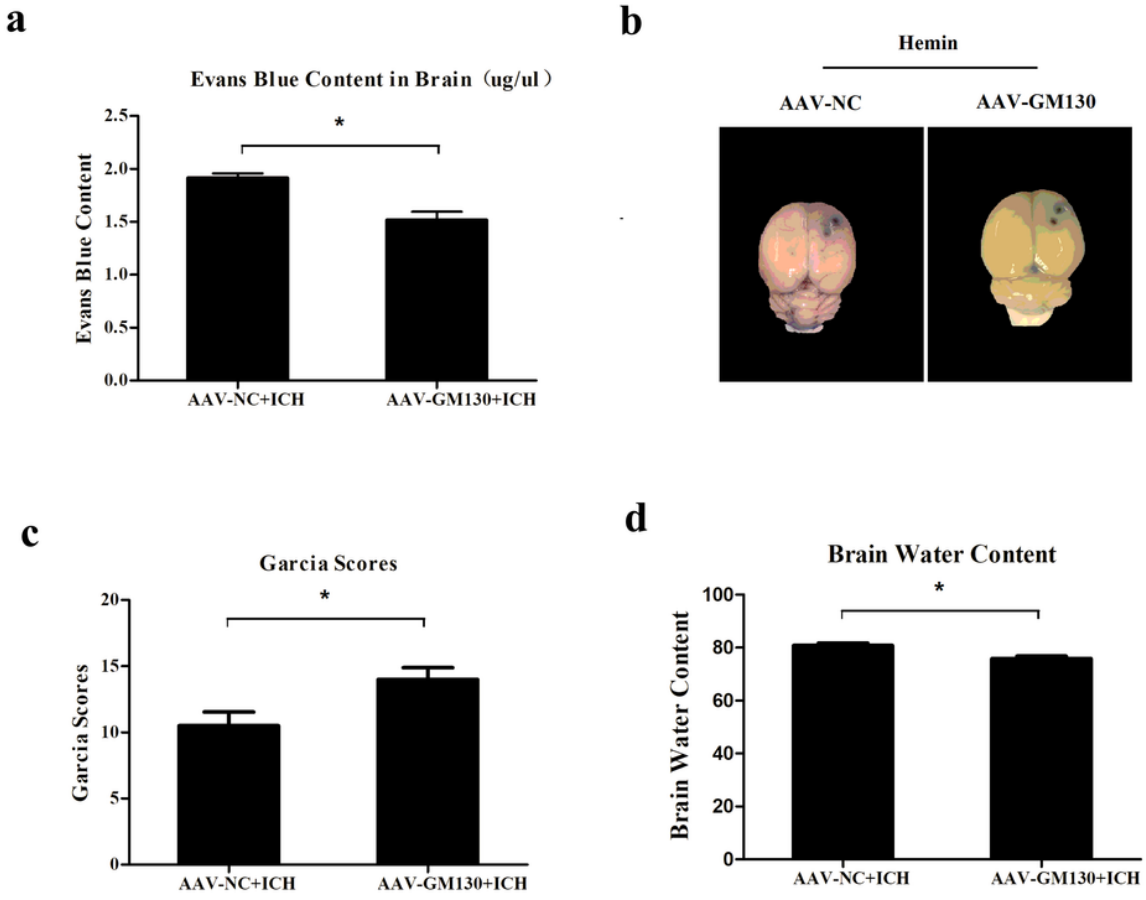


## Figure 8

Silencing GM130 increases blood-brain barrier disruption and aggravates brain edema and neurologic dysfunction after intracerebral hemorrhage. a. Evans blue extravasation assay from the cerebrum of rats (shown in b) from the sham group and intracerebral hemorrhage (ICH) group pre-treated with or without siGM130. (n = 3 per group) c. Garcia score in sham and ICH groups pre-treated with or without siGM130 (n = 6 per group). d. Water content in sham and ICH groups pre-treated with or without siGM130 (n = 6 per group). Data are presented as means ± standard deviation (SD). *p < 0.05.

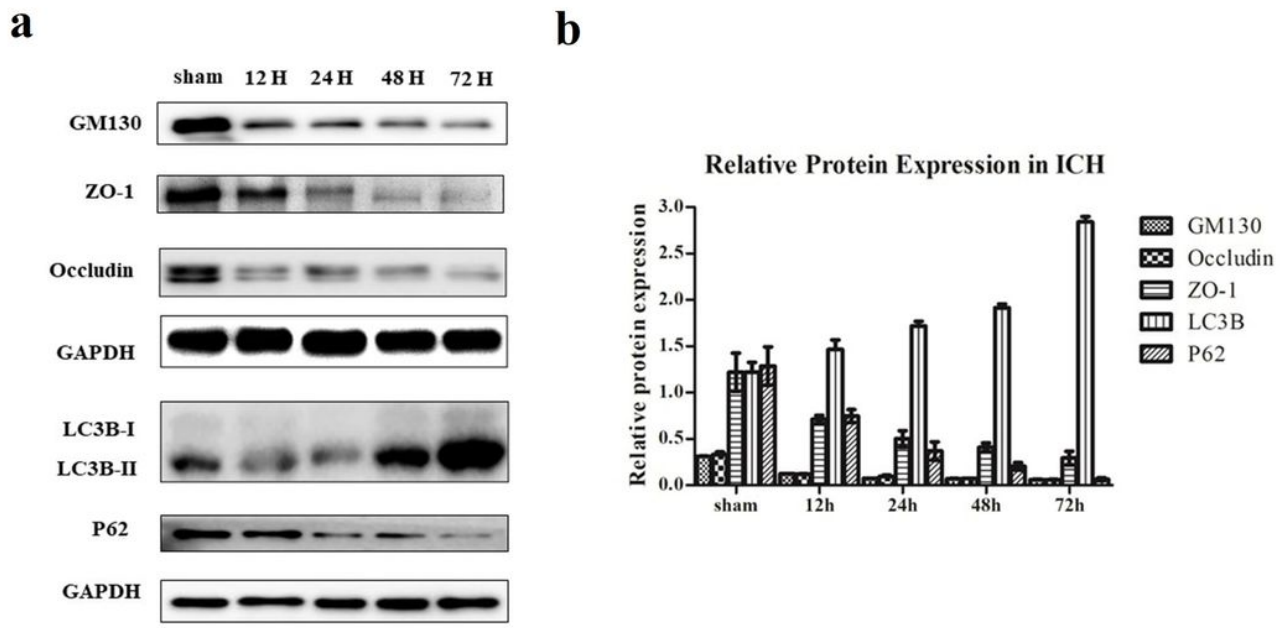


## Figure 9

Increasing time of intracerebral hemorrhage decreased GM130 and tight junction integrity and increased autophagy formation. a. Western blot showing GM130, occludin, ZO-1, LC3, and p62 expression in hemorrhaged rat brains of the sham and intracerebral hemorrhage (ICH) groups after 12, 24, 48, or 72 h (n = 6 per group). b. Quantification data are presented as means ± standard deviation (SD). *p < 0.05.

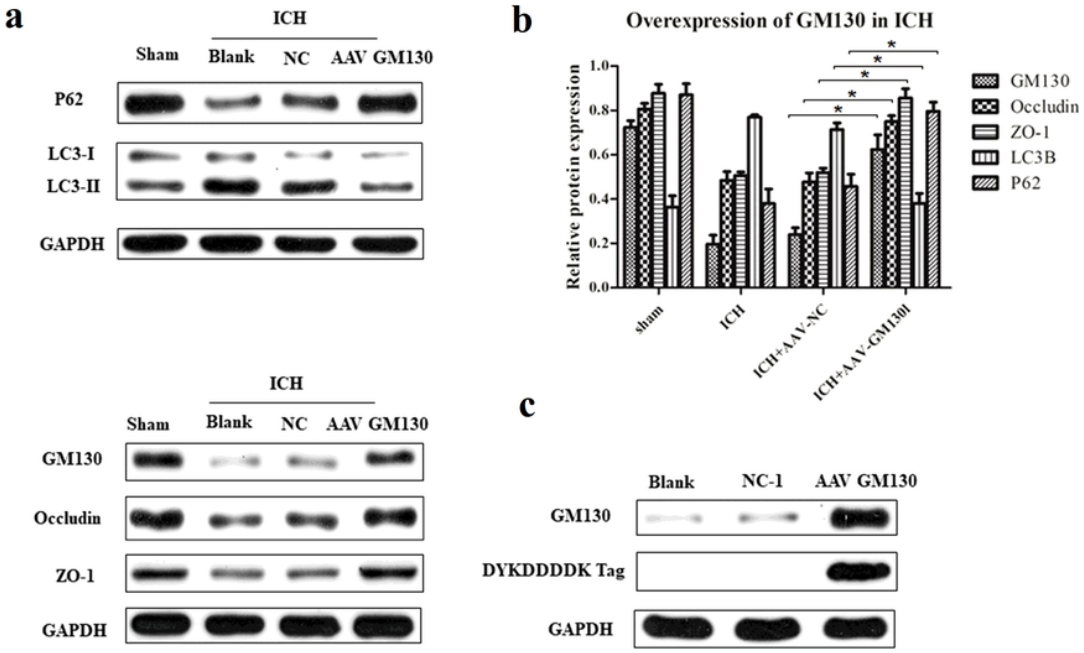


## Figure 10

AAV-GM130 has a neuroprotective effect on intracerebral hemorrhage via repairing tight junction protein expression. a. Western blot showing GM130, occludin, ZO-1, LC3, and p62 expression in hemorrhaged rat brains of the sham and intracerebral hemorrhage (ICH) group treated with saline, AAV-Control, or AAV-GM130 (n = 6 per group). b. Quantification data are presented as means ± standard deviation (SD). *p < 0.05. c. AAV-GM130 was successfully transfected into the rat brain.

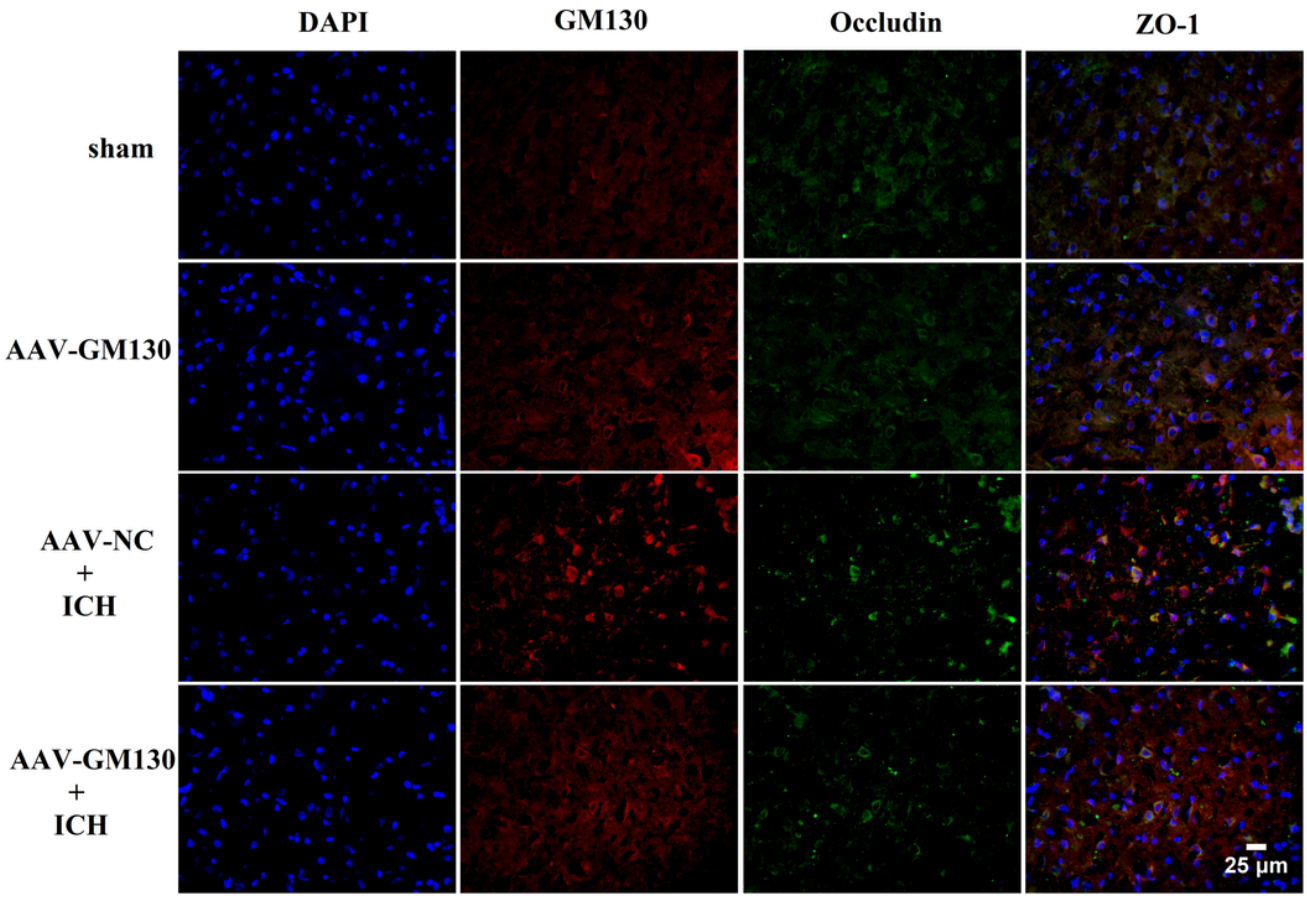


## Figure 11

Immunostaining of GM130 in the hemorrhaged rat brain. Immunostaining of GM130 and occludin in hemorrhaged rat brains of the sham and intracerebral hemorrhage (ICH) groups treated with saline, AAV-Control, or AAV-GM130 (n = 3 per group). Scale bar, 25 μm.

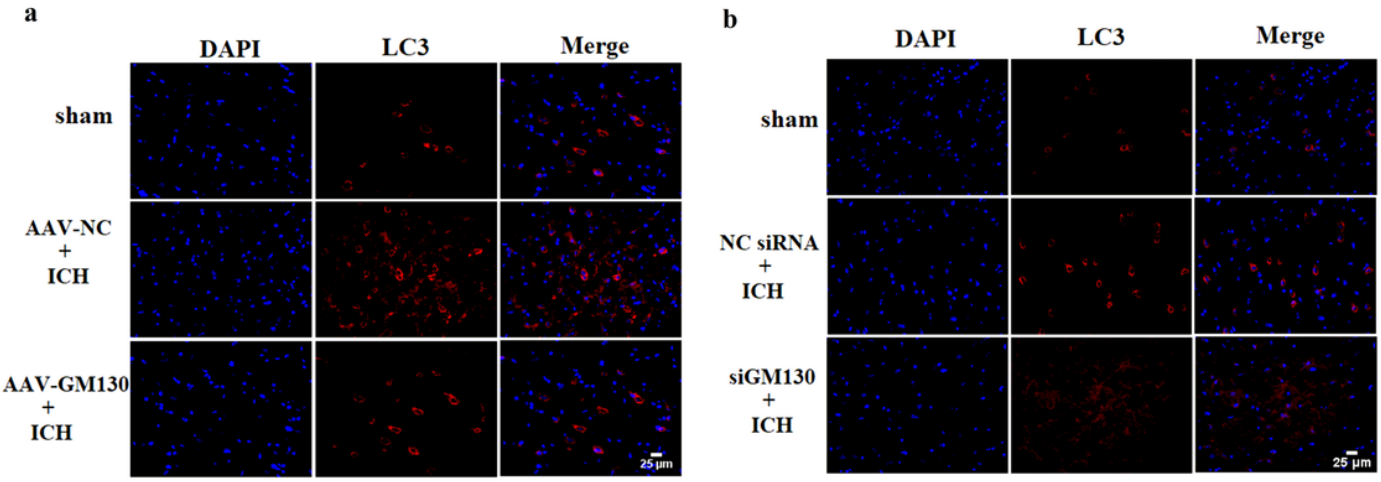

## Figure 12

Immunostaining of LC3 in the hemorrhaged rat brain. a. Immunostaining of LC3 in hemorrhaged rat brains of the sham and intracerebral hemorrhage (ICH) groups treated with saline, AAV-Control, or AAV-GM130 (n = 3 per group). b. Immunostaining of LC3 in hemorrhaged rat brains of the sham and ICH groups treated with saline, si-Control, or siGM130. Scale bar, 25 μm.

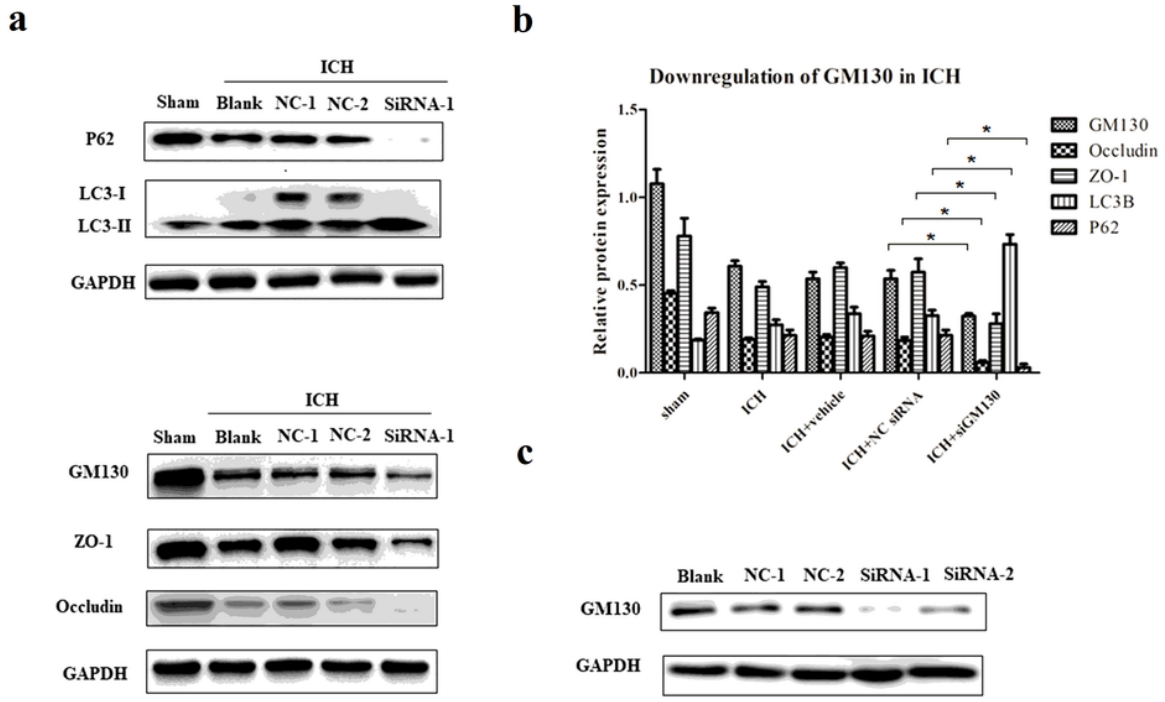


## Figure 13

Silencing GM130 promotes formation of autophagosomes and impairs tight junction proteins in hemorrhaged rat brains. a. Western blot showing GM130, occludin, ZO-1, LC3, and p62 expression in hemorrhaged rat brains of the sham and intracerebral hemorrhage (ICH) groups treated with saline, si-Control, or Si-GM130 (n = 6 per group). b. Quantification data are presented as means ± standard deviation (SD). *p < 0.05. c. siGM130 successfully silenced the expression of GM130 in the rat brain.

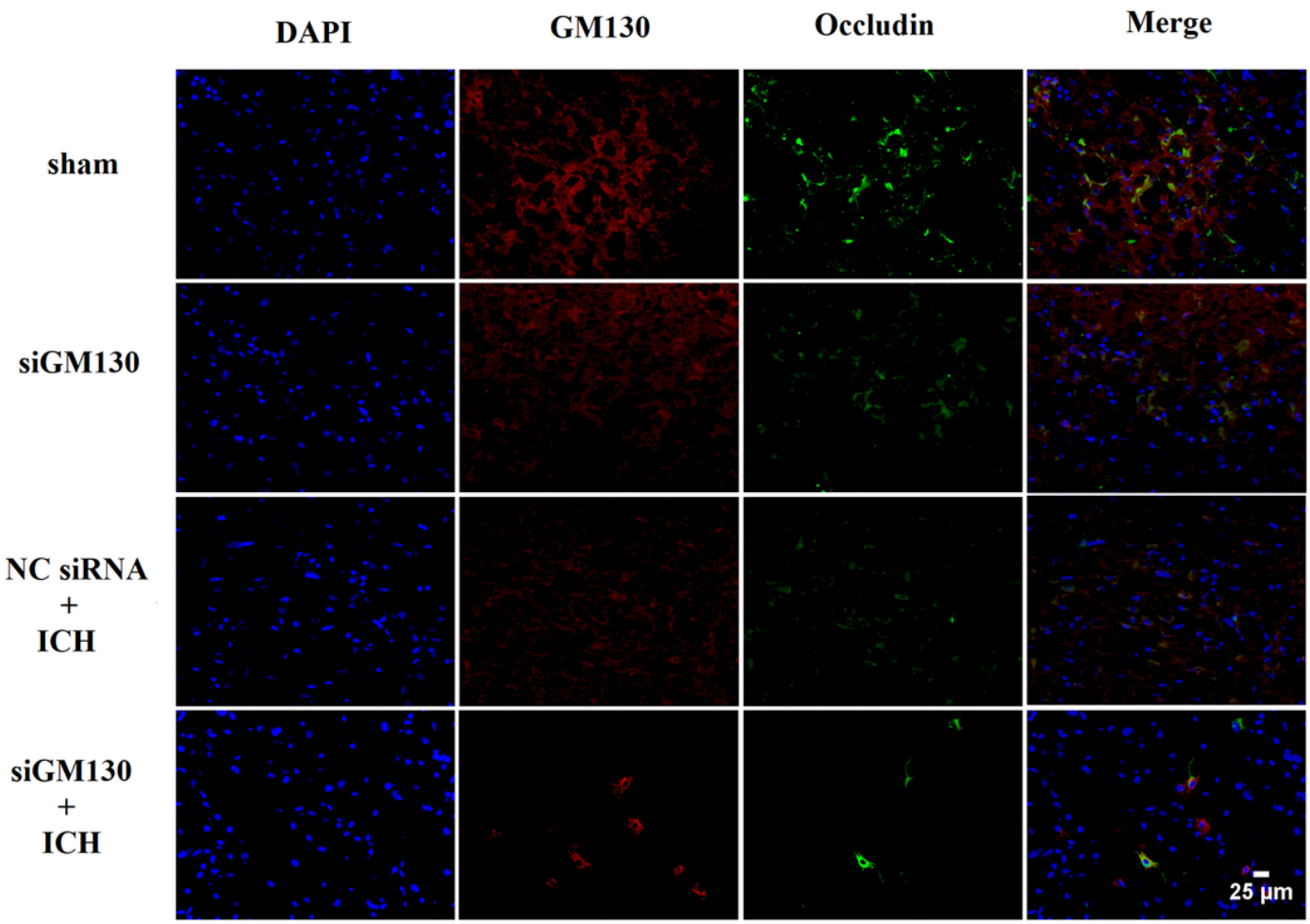


## Figure 14

Immunostaining of GM130 in the hemorrhaged rat brain. Immunostaining of GM130 and occludin in hemorrhaged rat brains of the sham and intracerebral hemorrhage (ICH) groups treated with saline, si-Control, or siGM130 (n = 3 per group). Scale bar, 25 μm.

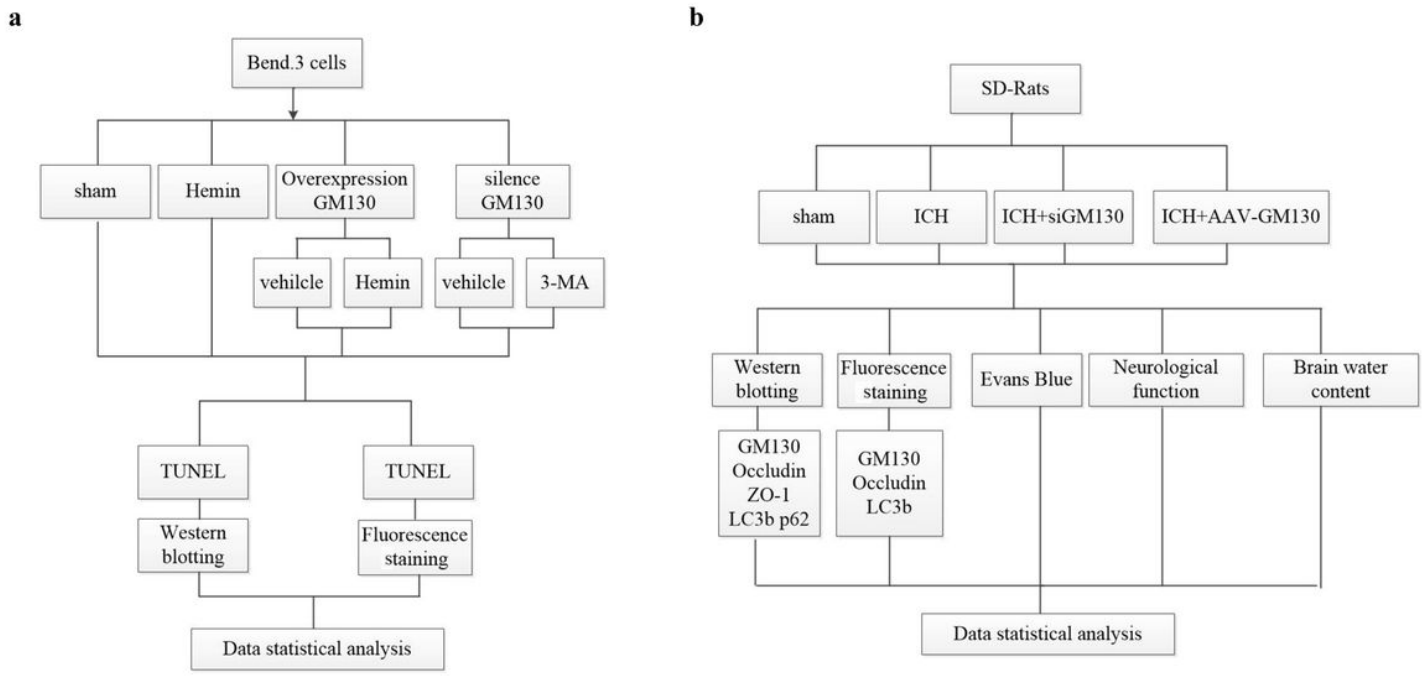


## Figure 15

Experimental designs. a. Experiment 1 was designed to investigate the effect of silencing or overexpression of GM130 on the blood brain barrier in vitro. b. Experiment 2 was designed to investigate the effect of silencing or overexpression of GM130 on the blood brain barrier in vivo.